Acta Cryst E CRYSTALLOGRAPHIC COMMUNICATIONS

ISSN 2056-9890

Polymorphism and Hirshfeld surface analysis of tetraoxa[2]perfluoroarene[2]triazine

Tadashi Kawasaki and Akiko Hori*

Department of Applied Chemistry, Graduate School of Engineering & Science, 307 Fukasaku, Minuma-ku, Saitama-shi, Saitama 337-8570, Japan. *Correspondence e-mail: ahori@shibaura-it.ac.jp

Received 21 February 2025
Accepted 28 February 2025

Edited by B. Therrien, University of Neuchâtel, Switzerland

Keywords: crystal structure; polymorphism; tetrafluorophenylene; triazine; Hirshfeld surface analysis.

CCDC references: 2427768; 2427767

Supporting information: this article has supporting information at journals.iucr.org/e

The title compound, tetraoxa[2]perfluoroarene[2]triazine ($C_{20}H_6F_8N_6O_6$), composed of two tetrafluorophenylene and two triazine moieties connected by four oxygen atoms, was crystallized *via* slow evaporation of a dichloromethane solution, yielding two polymorphs: block- (**I**) and plate-shaped (**II**) crystals. Polymorph **I** (triclinic, $P\overline{1}$, V = 516 Å^3 at 173 K) was previously reported by Yang *et al.* [(2015. *Org. Lett.* **15**, 4414–4417] whereas the newly identified polymorph **II** (triclinic, $P\overline{1}$, V = 1085 Å^3 at 100 K) shares the same space group but has a unit-cell volume twice as large, accommodating two symmetrically distinct molecules, *Molecule-1* and *Molecule-2*, with a different molecular arrangement. Since these crystals are expected to exhibit the characteristics of non-porous adaptive crystals, detailed analyses of intermolecular interactions were conducted, revealing that C—F···π-hole interactions are more pronounced in **II** than in **I**. Hirshfeld surface analysis at 100 K revealed that the primary contributions to the crystal packing in polymorph **I** were F···F (17.1%), F···H/H···F (21.5%), C···H/H···C (6.3%), C···F/F···C (4.5%) and C···O/O···C (9.2%) interactions, whereas in polymorph **II**, these interactions were F···F (9.9% and 10.0%), F···H/H···F (20.9% and 26.5%), C···H/H···C (6.3% and 2.9%), C···F/F···C (8.5% and 10.0%) and C···O/O···C (4.9% and 4.6%) for *Molecule-1* and *Molecule-2*, respectively. Powder X-ray diffraction analysis indicates that polymorph **I** is the more stable crystalline form, predominantly obtained through rapid precipitation or by grinding the crystals.

1. Chemical context

Polymorphism, the ability of a compound to crystallize in multiple forms, is significant for its implications in molecular recognition, separation processes, and the design of non-porous adaptive crystals (Jie *et al.*, 2018; Yan *et al.*, 2023). Among polymorphic systems, tetraoxa[4]arene derivatives, which feature aromatic rings linked by heteroatoms, stand out due to their structural flexibility and diversity. Tetraoxa[4]-arene, 2,4,6,8-tetraoxa-1,5(1,3),3,7(1,4)-tetrabenzenacyclo-octaphane (Zhou *et al.*, 2014), a cyclic molecule comprising four phenylene units bridged by oxygen atoms, is a notable example exhibiting polymorphism. Crystallization studies have shown that tetraoxa[4]arene forms block-shaped crystals (monoclinic, $P2_1/c$) and prismatic crystals (monoclinic, $P2_1/n$), each displaying distinct molecular arrangements and intermolecular interactions (Ishida *et al.*, 2024). These features, particularly its ability to form non-porous adaptive crystals, highlight its potential as a solid-state host framework with molecular recognition properties.

Accordingly, to investigate π-hole interactions in electron-deficient aromatic systems (Williams, 1993; Hori, 2012), we have focused on the title compound, a structurally related analogue of tetraoxa[4]arene in which the phenylene units are replaced by tetrafluorophenylene and triazine moieties (Yang

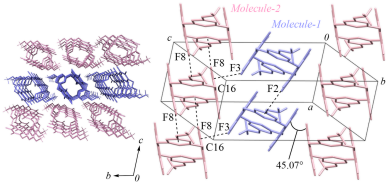

et al., 2013). This structural modification extends the chemical and structural diversity of tetraoxa[4]arene derivatives, enabling exploration of the effects of fluorination and triazine substitution as π-hole systems (Shimizu *et al.*, 2009; Salonen *et al.*, 2011; Wang *et al.*, 2015; Politzer *et al.*, 2021) on the crystal packing and intermolecular interactions. A previously reported polymorph of the title compound (triclinic, $P\overline{1}$) was noted for its potential adaptive crystal behavior. Inspired by the polymorphism observed in tetraoxa[4]arene, we investigated the crystallization of the title compound and identified not only the previously reported block-shaped crystals, but also a novel plate-like form. This plate polymorph retains the same space group, but exhibits a unit-cell volume twice as large, accommodating a distinct molecular arrangement. This study focuses on the crystallographic and structural characterization of the newly identified polymorph, aiming to elucidate its polymorphic behavior and intermolecular interactions. Through this investigation, we seek to provide insights into the relationship between molecular structure and polymorphism.

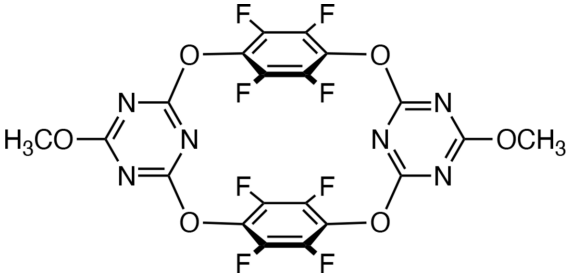

2. Structural commentary

The title compound was prepared following a reported method (Yang *et al.*, 2013) *via* a two-step coupling reaction between tetrafluorohydroquinone and 2,4-dichloro-6-methoxy-1,3,5-triazine. After thorough purification, crystallization from a CH_2Cl_2 solution *via* slow evaporation yielded colorless block-shaped crystals (**I**) as the primary polymorph and plate-shaped crystals (**II**) as the minor polymorph. Repeated optimization experiments demonstrated that **II** could also be obtained as the primary polymorph under slow evaporation of the solvent, being isolated as the major polymorph.

Single-crystal structure analysis confirmed the polymorphic nature of the compound; the major block-shaped polymorph **I** ($P\overline{1}$) corresponds to the crystal structure previously reported by Wang *et al.* (2015) while the minor plate-like polymorph **II** also crystallizes in the same space group, but with a unit-cell dimension doubled along the *c*-axis. Although both polymorphs share the same crystal system and are centrosymmetric, they differ in their molecular packing arrangements. To compare the intermolecular interactions, a structural analysis was conducted for both crystals at 100 K. Additionally, the thermal stability of each crystal system was evaluated by examining their structural parameters at room temperature. The *ORTEP* representations of **I** and **II** at 100 K, along with their atom-labeling schemes, are shown in Fig. 1.

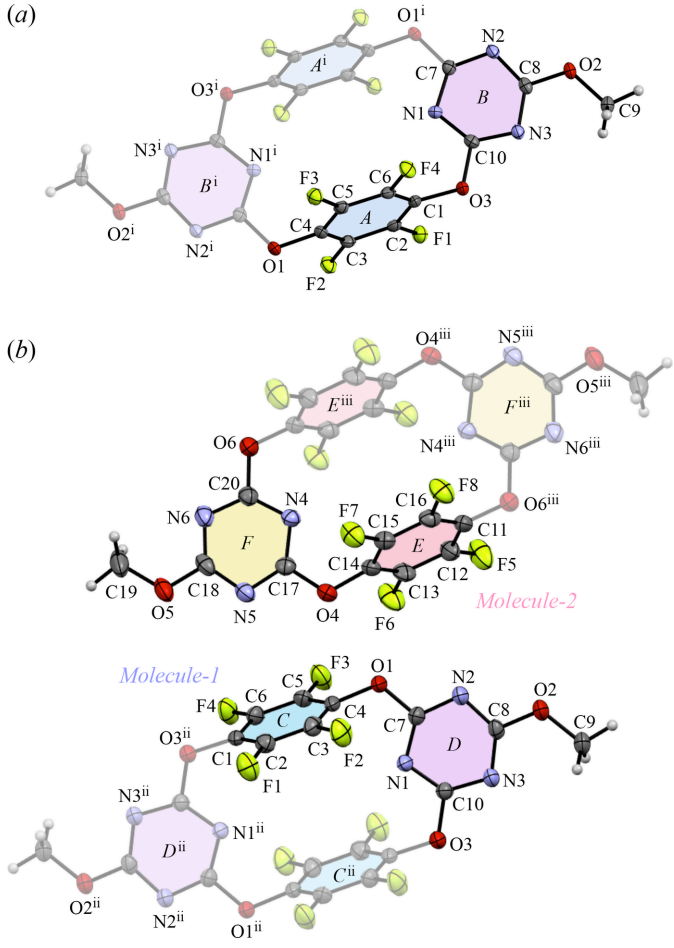

Figure 1
Molecular structure of (*a*) **I** and (*b*) **II** at 100 K, showing the atom-labeling schemes. Displacement ellipsoids are drawn at the 50% probability level. Color scheme: C, gray; F, green; N, blue; O, red. Symmetry codes: (i) $-x+1, -y+2, -z+1$; (ii) $-x, -y+1, -z+1$; (iii) $-x+1, -y+1, -z$.

In polymorph **I**, the unit cell contains two half-molecules as centrosymmetric units. The molecule is a cyclic structure in which two tetrafluorophenylene rings and two triazine rings are alternately connected by oxygen atoms, with its inversion center located at the midpoint between them (Fig. 1*a*). The average C—O bond lengths and C—O—C bond angles for the oxygen atoms (O1 and O3) in the macrocyclic framework are 1.38 Å and 116°, respectively, indicating single bonds and localized π electrons. In polymorph **II**, the unit cell contains four half-molecules, which are crystallographically independent and designated as *Molecule-1* and *Molecule-2* (Fig. 1*b*). The average C—O bond lengths and C—O—C bond angles of the framework are 1.37 Å and 116° for *Molecule-1* (O1 and O3), and 1.38 Å and 116° for *Molecule-2* (O4 and O6), respectively. Intramolecular repulsion between fluorine atoms on opposing tetrafluorophenylene groups, such as F1 (Ring-*A*) and F3 (Ring-A^i) [symmetry code: (i) $-x+1, -y+2, -z+1$], and between fluorine and nitrogen atoms on adjacent tetrafluorophenylene and triazine groups, such as F2 (Ring-*A*)$\cdots$N1 (Ring-*B*)$\cdots$F3 (Ring-*A*), contributes to the overall molecular shape. The structural overlay of the cyclic frameworks,

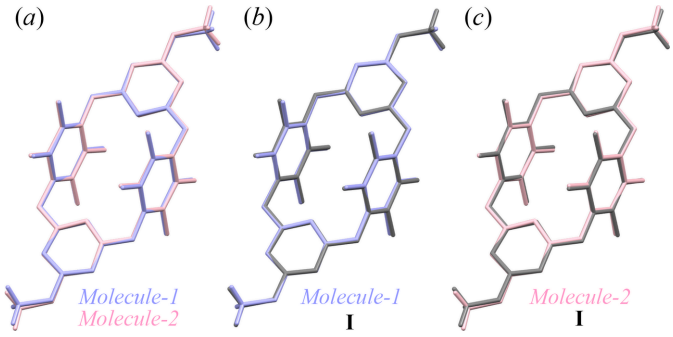

Figure 2
Structure overlays of the compound in the crystal of (*a*) *Molecule-1* (in blue) and *Molecule-2* (in pink) in **II**, (*b*) **I** (in gray) and *Molecule-1*, and (*c*) **I** (in gray) and *Molecule-2* at 100 K.

consisting of eighteen carbon, six nitrogen, and four oxygen atoms, of *Molecule-1* and *Molecule-2* gives an r.m.s. deviation of 0.0564 Å (Fig. 2). Similarly, the r.m.s. deviations for the structural overlays of the cyclic frameworks in polymorph **I** compared with *Molecule-1* and *Molecule-2* in polymorph **II** are 0.052 and 0.0836 Å, respectively. As with tetraoxa[4]arene, the molecular structures are nearly identical, suggesting that the polymorphism observed originates not from differences in molecular orientation, but rather from kinetically driven intermolecular interactions during the crystallization process.

3. Supramolecular features

The packing structure of polymorph **I** and its key intermolecular interactions are summarized in Fig. 3. The molecules are aligned parallel to the $(0\bar{1}1)$ plane, forming a linear channel structure along the *a*-axis direction (Fig. 3*a*). Void analysis using *Mercury* (Macrae *et al.*, 2020) revealed that the radius of this channel is approximately 0.6 Å, indicating that it is not large enough for molecular insertion. The dihedral angle between Ring-*A* and Ring-*B* was determined to be 76.22 (12)°, indicating that the opposing aromatic rings are positioned nearly parallel. Regarding intermolecular interactions, H···F interactions were identified between H9*A*···F3, H9*B*···F1, and H9*B*···F2, with respective distances of 2.437, 2.630, and 2.601 Å, respectively (Fig. 3*b*). Other common intermolecular interactions were scarcely detected in *PLATON* (Spek, 2020), while the short distances of C—H···π-hole, N···F, O···F, and F···F suggest that intermolecular electrostatic interactions contribute to the crystal packing.

The packing structures and the corresponding intermolecular interactions in **II** are shown in Fig. 4, where the two crystallographically independent molecules, *Molecule-1* and *Molecule-2*, are identified in blue and pink, respectively, each being composed of two half-molecules related by an inversion center [symmetry codes: (ii) $-x, -y+1, -z+1$; (iii) $-x+1, -y+1, -z$). The dihedral angles between the tetrafluorophenylene moieties of *Molecule-1* and *Molecule-2* are 45.07 (14)°, indicating a zigzag arrangement. Since both polymorphs **I** and **II** exhibit parallel π-hole planes within the molecules, the compound is expected to form a co-crystal through π-hole···π interactions with aromatic guests *via* both the triazine and tetrafluorophenylene rings (Williams, 2017). The stabilization of these structures can be attributed to electrostatic repulsions observed in both polymorphs; several notable intermolecular interactions were identified in **II**. The presence of C—F···π-hole interactions involving F2···C_g (Ring-*D*) and F8···C_g (Ring-*F*), as well as O···π-hole interactions observed between O5 and C_g (Ring-*D*), significantly contribute to the crystal packing: the intermolecular distances are 3.136 (2) and 2.977 (2) Å for C—F···π-hole, and 3.585 Å

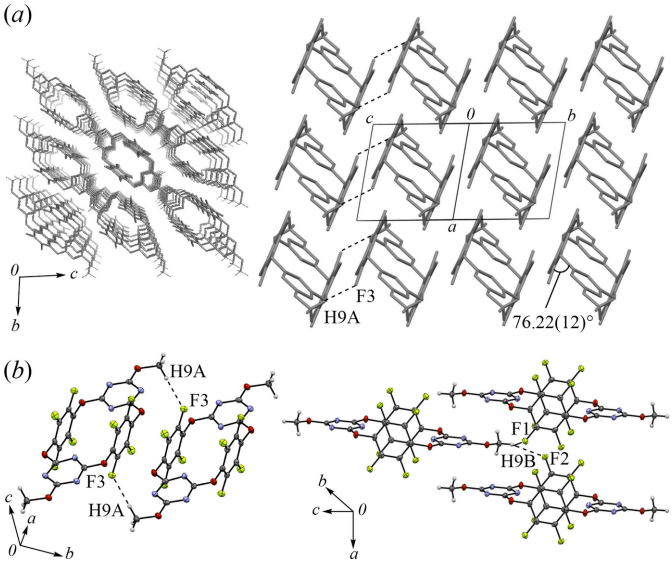

Figure 3
Partial packing views: (*a*) columnar arrangement along the *a*-axis (top view) and *bc*-direction (side view), (*b*) notable intermolecular H···F interactions in **I**.

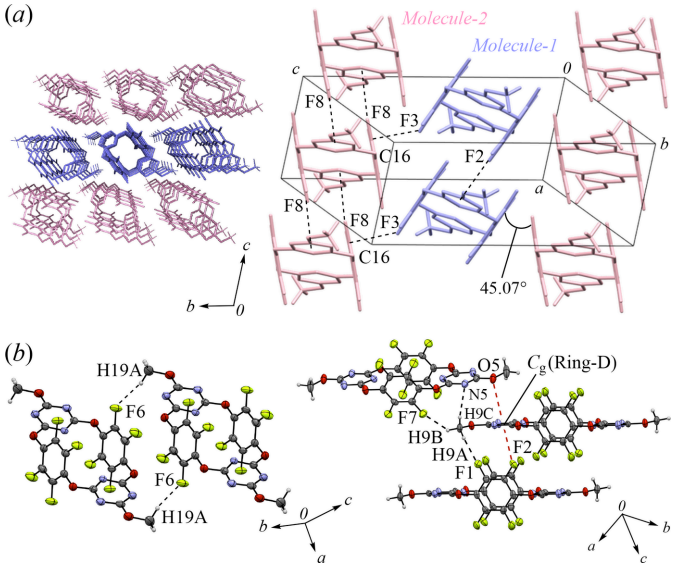

Figure 4
Partial packing views: (*a*) top and side views of the columnar arrangement along the *a*-axis, (*b*) notable intermolecular H···F, H···N, C—F···π-hole, and O···π-hole interactions in **II**.

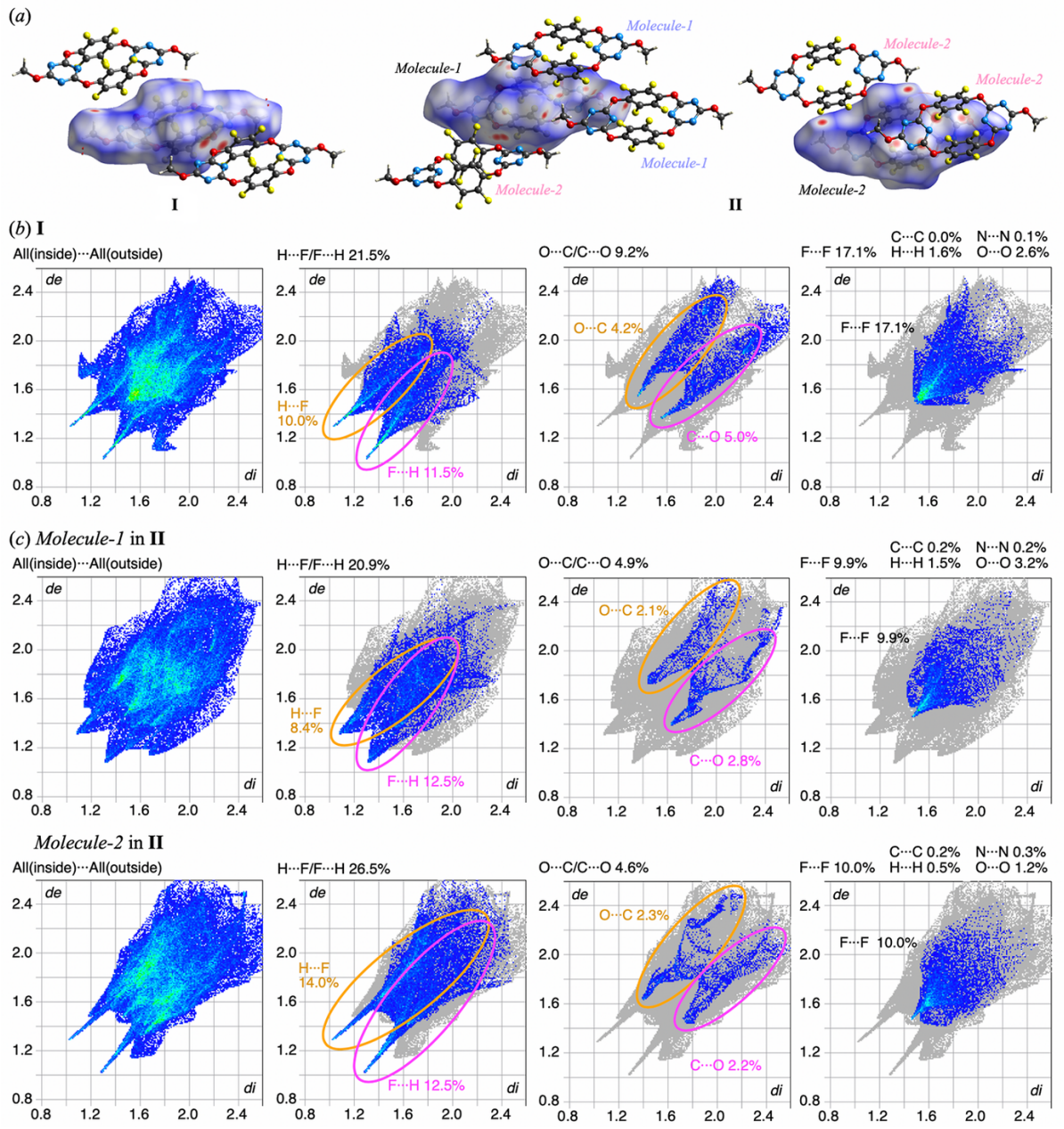

Figure 5
(*a*) Hirshfeld surface with d_{norm} of **I** and **II**. Fingerprint plots of (*b*) **I** and (*c*) **II**

for O···π-hole interactions. H···F interactions, such as H19*A*···F6, H9*A*···F1, and H9*B*···F7, and H···N interaction, H9*C*···N5, were observed with corresponding distances of 2.412, 2.500, 2.633, and 2.739 Å. Similar to **I**, polymorph **II** also forms a linear channel structure along the *a*-axis direction. Void analysis revealed that the channel radius is approximately 0.6 Å, indicating that it is not large enough for molecular insertion.

4. Hirshfeld surface analysis

To further investigate the strength of these interactions, Hirshfeld surface (HS) analysis was conducted (Hirshfeld, 1977; Spackman & Jayatilaka, 2009) using *Crystal Explorer 21.5* (Turner *et al.*, 2017). HS d_{norm} mapping of **I** and **II** (Fig. 5*a*) and fingerprint plots of **I** (Fig. 5*b*) confirmed that, in addition to the previously identified H···F/F···H interactions (21.5%), O···C/C···O interactions (9.2%) also play a significant role between the molecules. The C···O contact distance was measured at 3.227 (3) Å, which is the same of the sum of the van der Waals radii (3.22 Å). Although *PLATON* (Spek, 2020) did not explicitly classify this as a notable interaction, the adjacent carbon and oxygen atoms engage in C···O interactions, increasing the overall contribution of this interaction to the crystal packing stability. No π-hole···π-hole stacking was observed due to the 0% contribution of C···C contacts.

For HS analysis of *Molecule-1* and *Molecule-2* in polymorph **II** (Fig. 5*c*), C—F···π-hole interactions were prominently observed, with a higher contribution of C···F/F···C (8.5% and 10.0%, respectively) in **II** compared to **I** (4.5%). Fingerprint plots were analyzed to focus on C···F/F···C and N···F/F···N interactions between fluorine atoms of the inner and the outer molecules. This analysis was motivated by two key considerations: (i) the π-hole of the triazine ring consists of carbon and nitrogen atoms, and (ii) C···F and N···F interactions that do not involve the π-hole contribution were rarely observed. The results showed that both *Molecule-1* and *Molecule-2* exhibited a relatively high contribution of C···F and N···F interactions, further supporting the dominance of C—F···π-hole interactions in **II**. Additionally, the H···F/F···H interactions, which were prominently observed in **I**, exhibited a greater contribution in **II**. However, the contribution of C···O/O···C interactions decreased. HS mapping revealed an increase in the number of strong intermolecular interactions in **II**, suggesting that its lower symmetry arrangement resulted in a greater variety of intermolecular interactions, leading to a more dispersed distribution of interaction strengths.

5. Crystal growth and pXRD studies

To investigate the driving force behind the plate-like crystal growth in this structure, growth packing plane analyses were performed. As shown in Fig. 6*a*, the crystal grows along both the *a*- and *c*-axes. Along the *a*-axis, *Molecule-1* units are connected through C—F···π-hole interactions, while along the *c*-axis, *Molecule-1* and *Molecule-2* alternate, linked by the same type of interaction. In contrast, Fig. 6*b* illustrates that the *b*-axis is the smallest dimension of the plate, the unit-cell layers extend without significant intermolecular interactions. The formation of a distinct crystal system from polymorph **I** is attributed to the slow crystallization process, which enhances the dominance of C—F···π-hole interactions. At the same time, this process results in the emergence of growth-restricted planes, where these interactions are less effective. Consequently, the *b*-axis remains the direction of limited growth, leading to the formation of thin, plate-like crystals.

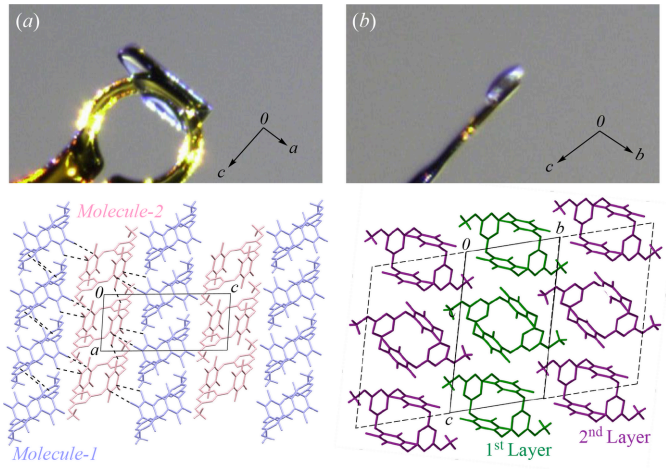

Figure 6
The crystal dimensions of polymorph **II**: views along (*a*) the *b*-axis and (*b*) the *a*-axis with the corresponding molecular arrangements.

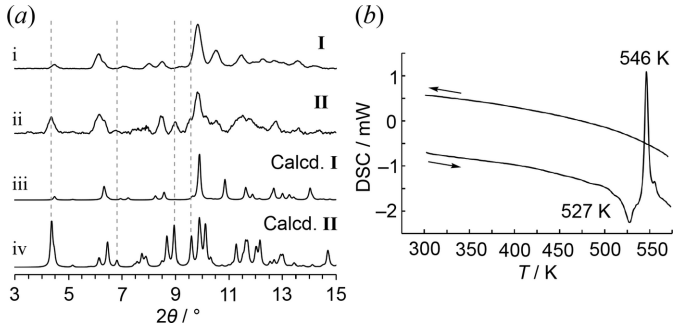

Figure 7
(*a*) pXRD patterns after grinding of (i) **I** and (ii) **II**; simulation patterns of (iii) **I** and (iv) **II** from scXRD, and (*b*) DSC of the title compound, scan rate: 10°C min^{-1}.

To verify whether polymorphs **I** and **II** undergo other crystalline phase transitions, pXRD measurements (similar to scXRD) were performed (Fig. 7*a*). The powder pattern of the prepared sample (pattern-i) closely matched the pXRD simulation derived from the single-crystal structure of **I**, with no detectable pattern corresponding to **II**. The observed broadening and peak shifts were attributed to measurements at room temperature and the use of the glass capillary method. During recrystallization, it was found that rapid precipitation favored the formation of the more densely packed crystal **I** (D_c = 1.875 g cm^{-3}) compared to **II** (D_c = 1.770 g cm^{-3}). In contrast, when the powder was dissolved in CH_2Cl_2 and allowed to concentrate as slowly as possible, the majority of the resulting crystals were identified as **II**. The pXRD measurement of this system produced a mixed pattern-ii, showing both **I** and **II** simulations. The reproducibility of this result suggests that the crystals underwent a phase transition upon grinding. A structurally similar tetraoxa[4]arene has been reported to undergo a phase transition at around 200 K for one of its polymorphic forms (Ishida, *et al.*, 2024). Therefore, the structure of **II** measured at 100 K was remeasured at r.t., but no significant changes in lattice parameters were observed. Similarly, no significant changes in lattice parameters were detected in **I** at both 100 K and r.t., as well as in the previously reported structure measured at 173 K. To further investigate, differential scanning calorimetry (DSC) was performed on the powdered sample (Fig. 7*b*), revealing an endothermic reaction around 527 K, suggesting melting. Additionally, an exothermic reaction was observed around 546 K; however, no peaks appeared during the cooling process, indicating that the compound had decomposed. Based on these findings, it was concluded that the compound does not undergo crystalline phase transitions upon temperature variation, and that the block-shaped polymorph **I** is generally the predominant form.

In summary, this study investigated the polymorphic behavior of the π-hole arene compound and its structural char-

Table 1
Experimental details.

	I	**II**
Crystal data		
Chemical formula	$C_{20}H_6F_8N_6O_6$	$C_{20}H_6F_8N_6O_6$
M_r	578.31	578.31
Crystal system, space group	Triclinic, $P\overline{1}$	Triclinic, $P\overline{1}$
Temperature (K)	100	100
a, b, c (Å)	7.1461 (19), 8.660 (2), 9.280 (3)	7.1729 (10), 9.7282 (12), 16.307 (2)
α, β, γ (°)	90.742 (9), 101.274 (9), 113.887 (9)	104.420 (4), 91.293 (5), 99.274 (4)
V (Å^3)	512.3 (2)	1085.3 (3)
Z	1	2
Radiation type	Mo $K\alpha$	Mo $K\alpha$
μ (mm^{-1})	0.19	0.18
Crystal size (mm)	0.18 × 0.12 × 0.06	0.25 × 0.19 × 0.09
Data collection		
Diffractometer	Bruker D8 Goniometer	Bruker D8 Goniometer
Absorption correction	Multi-scan (*SADABS*; Krause *et al.*, 2015)	Multi-scan (*SADABS*; Krause *et al.*, 2015)
T_{min}, T_{max}	0.84, 0.99	0.74, 0.98
No. of measured, independent and observed [$I > 2\sigma(I)$] reflections	3886, 1723, 1324	10388, 3800, 2824
R_{int}	0.030	0.053
$(\sin\theta/\lambda)_{max}$ (Å^{-1})	0.595	0.595
Refinement		
$R[F^2 > 2\sigma(F^2)]$, $wR(F^2)$, S	0.038, 0.092, 1.07	0.047, 0.130, 1.04
No. of reflections	1723	3800
No. of parameters	182	364
H-atom treatment	H-atom parameters constrained	H-atom parameters constrained
$\Delta\rho_{max}$, $\Delta\rho_{min}$ (e Å^{-3})	0.22, −0.28	0.26, −0.24

Computer programs: *APEX5* and *SAINT* (Bruker, 2019), *SHELXT2018/2* (Sheldrick, 2015*a*), *SHELXL2019/1* (Sheldrick, 2015*b*), *ShelXle* (Hübschle *et al.*, 2015) and *Mercury* (Macrae *et al.*, 2020).

acteristics. Single-crystal analysis confirmed two polymorphs (**I** and **II**), both in the triclinic $P\overline{1}$ space group but with different unit-cell dimensions. While polymorph **I** corresponds to a previously reported structure, polymorph **II** has a doubled unit cell and two independent molecules (*Molecule-1* and *Molecule-2*). C—F···π-hole interactions were found to be the dominant stabilizing force in both polymorphs. In **I**, these interactions contribute to a linear channel structure along the *a*-axis direction, with H···F interactions also playing a role. In **II**, C—F···π-hole interactions primarily link *Molecule-1* and *Molecule-2* along the *c*-axis, while H···F interactions show a higher contribution than in **I**. HS analysis further revealed C···F and N···F interactions, supporting the influence of triazine-based π-hole interactions. Growth-plane analysis indicated that slow crystallization enhances C—F···π-hole interactions, leading to plate-like crystal formation. These findings underscore the crucial role of π-hole interactions in crystal packing and polymorphism, providing insights into molecular recognition and crystal engineering.

6. Refinement

Crystal data, data collection and structure refinement details are summarized in Table 1. H atoms were placed in geometrically idealized positions and refined as riding atoms with C—H = 0.95 Å and 0.98 Å for aromatic and aliphatic hydrogen, with $U_{iso}(H) = 1.2U_{eq}(C)$.

Funding information

Funding for this research was provided by: JSPS KAKENHI (grant No. 23 K21122).

References

Bruker (2019). *APEX5* and *SAINT*. Bruker AXS Inc., Madison, Wisconsin, USA.
Hirshfeld, F. L. (1977). *Theor. Chim. Acta*, **44**, 129–138.
Hori, A. (2012). *Frontiers in Crystal Engineering, Vol. III*, pp. 163–185. New York: John Wiley & Sons.
Hübschle, C. B., Sheldrick, G. M. & Dittrich, B. (2011). *J. Appl. Cryst.* **44**, 1281–1284.
Ishida, Y., Kawasaki, T. & Hori, A. (2024). *Crystals*, **14**, 1032.
Jie, K., Zhou, Y., Li, E. & Huang, F. (2018). *Acc. Chem. Res.* **51**, 2064–2072.
Krause, L., Herbst-Irmer, R., Sheldrick, G. M. & Stalke, D. (2015). *J. Appl. Cryst.* **48**, 3–10.
Macrae, C. F., Sovago, I., Cottrell, S. J., Galek, P. T. A., McCabe, P., Pidcock, E., Platings, M., Shields, G. P., Stevens, J. S., Towler, M. & Wood, P. A. (2020). *J. Appl. Cryst.* **53**, 226–235.
Politzer, P., Murray, J. S. & Clark, T. (2021). *Phys. Chem. Chem. Phys.* **23**, 16458–16468.
Salonen, L. M., Ellermann, M. & Diederich, F. (2011). *Angew. Chem. Int. Ed.* **50**, 4808–4842.
Sheldrick, G. M. (2015*a*). *Acta Cryst.* A**71**, 3–8.
Sheldrick, G. M. (2015*b*). *Acta Cryst.* C**71**, 3–8.
Shimizu, K., Costa Gomes, M. F., Pádua, A. A. H., Rebelo, L. P. N. & Canongia Lopes, J. N. (2009). *J. Phys. Chem. B*, **113**, 9894–9900.
Spackman, M. A. & Jayatilaka, D. (2009). *CrystEngComm*, **11**, 19–32.
Spek, A. L. (2020). *Acta Cryst.* E**76**, 1–11.

Turner, M. J., McKinnon, J. J., Wolff, S. K., Grimwood, D. J., Spackman, P. R., Jayatilaka, D. & Spackman, M. A. (2017). *Crystal Explorer 17*. The University of Western Australia.
Wang, H., Li, C., Wang, W. & Jin, W. J. (2015). *Phys. Chem. Chem. Phys.* **17**, 20636–20646.
Williams, J. H. (1993). *Acc. Chem. Res.* **26**, 593–598.
Williams, J. H. (2017). *Crystal Engineering: How Molecules Build Solids.* San Rafael, California: Morgan & Claypool Publishers.
Yan, M., Wang, Y., Chen, J. & Zhou, J. (2023). *Chem. Soc. Rev*. **52**, 6075–6119.
Yang, C., Chen, Y., Wang, D.-X., Zhao, L. & Wang, M.-X. (2013). *Org. Lett.* **15**, 4414–4417.
Zhou, Q., Su, L., Jiang, T., Zhang, B., Chen, R., Jiang, H., Ye, Y., Zhu, M., Han, D., Shen, J., Dai, G. & Li, Z. (2014). *Tetrahedron*, **70**, 1125–1132.

supporting information

Acta Cryst. (2025). E**81**, 289-295 [https://doi.org/10.1107/S205698902500194X]

Polymorphism and Hirshfeld surface analysis of tetraoxa[2]perfluoroarene[2]triazine

Tadashi Kawasaki and Akiko Hori

Computing details

Tetraoxa[2]perfluoroarene[2]triazine (I)

Crystal data

$C_{20}H_6F_8N_6O_6$
M_r = 578.31
Triclinic, $P\overline{1}$
a = 7.1461 (19) Å
b = 8.660 (2) Å
c = 9.280 (3) Å
α = 90.742 (9)°
β = 101.274 (9)°
γ = 113.887 (9)°
V = 512.3 (2) Å^3
Z = 1
$F(000)$ = 288
D_x = 1.875 Mg m^{-3}
Mo $K\alpha$ radiation, λ = 0.71073 Å
Cell parameters from 1960 reflections
θ = 3.2–26.3°
μ = 0.19 mm^{-1}
T = 100 K
Block, colourless
0.18 × 0.12 × 0.06 mm

Data collection

Bruker D8 Goniometer diffractometer
Detector resolution: 7.3910 pixels mm^{-1}
φ and ω scans
Absorption correction: multi-scan (SADABS; Krause et al., 2015)
T_{min} = 0.84, T_{max} = 0.99
3886 measured reflections
1723 independent reflections
1324 reflections with $I > 2\sigma(I)$
R_{int} = 0.030
θ_{max} = 25.0°, θ_{min} = 3.2°
h = −8→8
k = −9→10
l = −11→10

Refinement

Refinement on F^2
Least-squares matrix: full
$R[F^2 > 2\sigma(F^2)]$ = 0.038
$wR(F^2)$ = 0.092
S = 1.07
1723 reflections
182 parameters
0 restraints
Hydrogen site location: inferred from neighbouring sites
H-atom parameters constrained
$w = 1/[\sigma^2(F_o^2) + (0.0367P)^2 + 0.2238P]$ where $P = (F_o^2 + 2F_c^2)/3$
$(\Delta/\sigma)_{max} < 0.001$
$\Delta\rho_{max}$ = 0.22 e Å^{-3}
$\Delta\rho_{min}$ = −0.28 e Å^{-3}

Special details

Geometry. All esds (except the esd in the dihedral angle between two l.s. planes) are estimated using the full covariance matrix. The cell esds are taken into account individually in the estimation of esds in distances, angles and torsion angles; correlations between esds in cell parameters are only used when they are defined by crystal symmetry. An approximate (isotropic) treatment of cell esds is used for estimating esds involving l.s. planes.

Fractional atomic coordinates and isotropic or equivalent isotropic displacement parameters (Å²)

	x	*y*	*z*	U_{iso}*/U_{eq}
C1	0.2310 (4)	0.6873 (3)	0.4991 (2)	0.0184 (5)
C2	0.0922 (4)	0.7559 (3)	0.5196 (2)	0.0182 (5)
C3	0.1420 (4)	0.8726 (3)	0.6386 (2)	0.0183 (5)
C4	0.3323 (4)	0.9251 (3)	0.7362 (2)	0.0181 (5)
C5	0.4723 (4)	0.8573 (3)	0.7158 (2)	0.0180 (5)
C6	0.4211 (4)	0.7375 (3)	0.5989 (2)	0.0184 (5)
C7	0.4728 (4)	0.7988 (3)	0.1483 (2)	0.0172 (5)
C8	0.2802 (4)	0.5391 (3)	0.0409 (2)	0.0174 (5)
C9	0.0875 (4)	0.2548 (3)	−0.0668 (3)	0.0210 (6)
H9A	0.159037	0.207379	0.008882	0.032*
H9B	0.050618	0.188273	−0.162360	0.032*
H9C	−0.040371	0.250658	−0.040013	0.032*
C10	0.2633 (4)	0.6098 (3)	0.2654 (2)	0.0174 (5)
F1	−0.0935 (2)	0.70620 (17)	0.42333 (14)	0.0232 (4)
F2	0.0058 (2)	0.93768 (17)	0.65671 (14)	0.0237 (4)
F3	0.6620 (2)	0.91391 (17)	0.80696 (14)	0.0226 (3)
F4	0.5565 (2)	0.67242 (18)	0.57993 (15)	0.0256 (4)
N1	0.4026 (3)	0.7671 (2)	0.2726 (2)	0.0166 (4)
N2	0.4183 (3)	0.6951 (2)	0.0277 (2)	0.0176 (5)
N3	0.1943 (3)	0.4860 (2)	0.1569 (2)	0.0181 (5)
O1	0.3814 (2)	1.0421 (2)	0.85763 (16)	0.0197 (4)
O2	0.2255 (2)	0.4297 (2)	−0.07699 (16)	0.0199 (4)
O3	0.1720 (2)	0.5621 (2)	0.38295 (17)	0.0211 (4)

Atomic displacement parameters (Å²)

	U^{11}	U^{22}	U^{33}	U^{12}	U^{13}	U^{23}
C1	0.0221 (14)	0.0125 (12)	0.0173 (12)	0.0017 (11)	0.0093 (10)	0.0010 (10)
C2	0.0193 (13)	0.0153 (12)	0.0159 (12)	0.0019 (11)	0.0063 (10)	0.0045 (10)
C3	0.0187 (13)	0.0180 (13)	0.0215 (13)	0.0081 (11)	0.0105 (10)	0.0047 (10)
C4	0.0212 (14)	0.0171 (13)	0.0139 (12)	0.0047 (11)	0.0066 (10)	0.0008 (10)
C5	0.0193 (13)	0.0173 (13)	0.0158 (12)	0.0053 (11)	0.0048 (10)	0.0050 (10)
C6	0.0192 (13)	0.0162 (13)	0.0224 (13)	0.0069 (11)	0.0110 (10)	0.0056 (10)
C7	0.0170 (13)	0.0166 (13)	0.0192 (13)	0.0082 (11)	0.0037 (10)	0.0015 (10)
C8	0.0181 (13)	0.0209 (13)	0.0150 (12)	0.0114 (11)	0.0004 (10)	−0.0017 (10)
C9	0.0228 (13)	0.0165 (13)	0.0214 (13)	0.0068 (11)	0.0027 (10)	−0.0027 (10)
C10	0.0184 (13)	0.0204 (14)	0.0156 (12)	0.0094 (12)	0.0057 (10)	0.0019 (10)
F1	0.0210 (8)	0.0241 (8)	0.0197 (7)	0.0062 (7)	0.0008 (6)	−0.0013 (6)
F2	0.0236 (8)	0.0250 (8)	0.0256 (7)	0.0126 (7)	0.0066 (6)	−0.0017 (6)

F3	0.0209 (8)	0.0252 (8)	0.0199 (7)	0.0089 (7)	0.0023 (6)	0.0002 (6)
F4	0.0264 (8)	0.0252 (8)	0.0298 (8)	0.0140 (7)	0.0097 (6)	−0.0012 (6)
N1	0.0181 (11)	0.0158 (11)	0.0160 (10)	0.0055 (9)	0.0069 (8)	0.0022 (8)
N2	0.0197 (11)	0.0179 (11)	0.0159 (10)	0.0083 (9)	0.0046 (8)	−0.0012 (8)
N3	0.0200 (11)	0.0171 (11)	0.0169 (10)	0.0077 (9)	0.0038 (8)	−0.0016 (8)
O1	0.0240 (9)	0.0178 (9)	0.0148 (8)	0.0046 (8)	0.0078 (7)	−0.0023 (7)
O2	0.0236 (10)	0.0175 (9)	0.0171 (8)	0.0074 (8)	0.0038 (7)	−0.0042 (7)
O3	0.0255 (10)	0.0156 (9)	0.0175 (8)	0.0022 (8)	0.0087 (7)	−0.0025 (7)

Geometric parameters (Å, º)

C1—C6	1.382 (3)	C6—F4	1.338 (2)
C1—C2	1.386 (3)	C7—N2	1.315 (3)
C1—O3	1.392 (3)	C7—N1	1.334 (3)
C2—F1	1.345 (3)	C7—O1^{i}	1.360 (3)
C2—C3	1.376 (3)	C8—O2	1.324 (2)
C3—F2	1.342 (2)	C8—N2	1.337 (3)
C3—C4	1.372 (3)	C8—N3	1.338 (3)
C4—C5	1.389 (3)	C9—O2	1.451 (3)
C4—O1	1.396 (2)	C10—N1	1.313 (3)
C5—F3	1.340 (3)	C10—N3	1.325 (3)
C5—C6	1.377 (3)	C10—O3	1.364 (3)
C6—C1—C2	119.53 (19)	C5—C6—C1	119.8 (2)
C6—C1—O3	120.98 (19)	N2—C7—N1	128.3 (2)
C2—C1—O3	119.4 (2)	N2—C7—O1^{i}	114.5 (2)
F1—C2—C3	119.9 (2)	N1—C7—O1^{i}	117.21 (19)
F1—C2—C1	119.63 (19)	O2—C8—N2	114.0 (2)
C3—C2—C1	120.5 (2)	O2—C8—N3	118.8 (2)
F2—C3—C4	120.23 (19)	N2—C8—N3	127.23 (19)
F2—C3—C2	119.7 (2)	N1—C10—N3	129.0 (2)
C4—C3—C2	120.1 (2)	N1—C10—O3	117.82 (19)
C3—C4—C5	119.6 (2)	N3—C10—O3	113.2 (2)
C3—C4—O1	119.94 (19)	C10—N1—C7	111.66 (19)
C5—C4—O1	120.39 (19)	C7—N2—C8	112.2 (2)
F3—C5—C6	119.70 (19)	C10—N3—C8	111.6 (2)
F3—C5—C4	119.79 (19)	C7^{i}—O1—C4	116.00 (18)
C6—C5—C4	120.4 (2)	C8—O2—C9	117.07 (18)
F4—C6—C5	120.2 (2)	C10—O3—C1	116.55 (18)
F4—C6—C1	120.02 (19)		
C6—C1—C2—F1	−179.5 (2)	C2—C1—C6—C5	−1.2 (4)
O3—C1—C2—F1	−3.0 (3)	O3—C1—C6—C5	−177.7 (2)
C6—C1—C2—C3	−0.3 (4)	N3—C10—N1—C7	2.1 (3)
O3—C1—C2—C3	176.2 (2)	O3—C10—N1—C7	−177.36 (18)
F1—C2—C3—F2	−0.8 (3)	N2—C7—N1—C10	0.6 (3)
C1—C2—C3—F2	180.0 (2)	O1^{i}—C7—N1—C10	−179.86 (19)
F1—C2—C3—C4	−179.3 (2)	N1—C7—N2—C8	−2.5 (3)

C1—C2—C3—C4	1.5 (4)	O1^{i}—C7—N2—C8	177.90 (18)
F2—C3—C4—C5	−179.7 (2)	O2—C8—N2—C7	−178.34 (18)
C2—C3—C4—C5	−1.2 (4)	N3—C8—N2—C7	2.4 (3)
F2—C3—C4—O1	2.2 (3)	N1—C10—N3—C8	−2.2 (3)
C2—C3—C4—O1	−179.3 (2)	O3—C10—N3—C8	177.27 (18)
C3—C4—C5—F3	176.9 (2)	O2—C8—N3—C10	−179.58 (19)
O1—C4—C5—F3	−5.0 (3)	N2—C8—N3—C10	−0.3 (3)
C3—C4—C5—C6	−0.3 (4)	C3—C4—O1—C7^{i}	−108.0 (3)
O1—C4—C5—C6	177.8 (2)	C5—C4—O1—C7^{i}	74.0 (3)
F3—C5—C6—F4	2.9 (3)	N2—C8—O2—C9	175.75 (18)
C4—C5—C6—F4	−179.9 (2)	N3—C8—O2—C9	−4.9 (3)
F3—C5—C6—C1	−175.7 (2)	N1—C10—O3—C1	1.8 (3)
C4—C5—C6—C1	1.5 (4)	N3—C10—O3—C1	−177.71 (18)
C2—C1—C6—F4	−179.8 (2)	C6—C1—O3—C10	−77.2 (3)
O3—C1—C6—F4	3.7 (4)	C2—C1—O3—C10	106.4 (2)

Symmetry code: (i) −*x*+1, −*y*+2, −*z*+1.

(II)

Crystal data

$C_{20}H_6F_8N_6O_6$
M_r = 578.31
Triclinic, $P\overline{1}$
a = 7.1729 (10) Å
b = 9.7282 (12) Å
c = 16.307 (2) Å
α = 104.420 (4)°
β = 91.293 (5)°
γ = 99.274 (4)°
V = 1085.3 (3) Å^3
Z = 2
F(000) = 576
D_x = 1.770 Mg m^{-3}
Mo *Kα* radiation, *λ* = 0.71073 Å
Cell parameters from 3736 reflections
θ = 2.2–25.3°
μ = 0.18 mm^{-1}
T = 100 K
Prismatic, colourless
0.25 × 0.19 × 0.09 mm

Data collection

Bruker D8 Goniometer diffractometer
Detector resolution: 7.3910 pixels mm^{-1}
φ and *ω* scans
Absorption correction: multi-scan (SADABS; Krause et al., 2015)
T_{min} = 0.74, T_{max} = 0.98
10388 measured reflections
3800 independent reflections
2824 reflections with $I > 2\sigma(I)$
R_{int} = 0.053
θ_{max} = 25.0°, θ_{min} = 2.6°
h = −8→7
k = −11→11
l = −19→17

Refinement

Refinement on F^2
Least-squares matrix: full
$R[F^2 > 2\sigma(F^2)]$ = 0.047
$wR(F^2)$ = 0.130
S = 1.03
3800 reflections
364 parameters
0 restraints
Hydrogen site location: inferred from neighbouring sites
H-atom parameters constrained
$w = 1/[\sigma^2(F_o^2) + (0.0502P)^2 + 0.5197P]$ where $P = (F_o^2 + 2F_c^2)/3$
$(\Delta/\sigma)_{max} < 0.001$
$\Delta\rho_{max}$ = 0.26 e Å^{-3}
$\Delta\rho_{min}$ = −0.24 e Å^{-3}
Extinction correction: *SHELXL2019/1* (Sheldrick, 2015b), $Fc^*=kFc[1+0.001xFc^2\lambda^3/\sin(2\theta)]^{-1/4}$
Extinction coefficient: 0.011 (2)

Special details

Geometry. All esds (except the esd in the dihedral angle between two l.s. planes) are estimated using the full covariance matrix. The cell esds are taken into account individually in the estimation of esds in distances, angles and torsion angles; correlations between esds in cell parameters are only used when they are defined by crystal symmetry. An approximate (isotropic) treatment of cell esds is used for estimating esds involving l.s. planes.

Fractional atomic coordinates and isotropic or equivalent isotropic displacement parameters (Å²)

	x	*y*	*z*	U_{iso}*/U_{eq}
C1	−0.0322 (4)	0.7241 (3)	0.43944 (16)	0.0287 (6)
C2	0.1465 (4)	0.7223 (3)	0.47154 (18)	0.0330 (6)
C3	0.2460 (4)	0.6168 (3)	0.43252 (18)	0.0333 (6)
C4	0.1702 (4)	0.5124 (3)	0.36165 (17)	0.0304 (6)
C5	−0.0089 (4)	0.5143 (3)	0.32978 (16)	0.0328 (6)
C6	−0.1094 (4)	0.6188 (3)	0.36824 (17)	0.0321 (6)
C7	0.2848 (4)	0.2983 (3)	0.35344 (16)	0.0300 (6)
C8	0.3974 (4)	0.1003 (3)	0.34991 (16)	0.0274 (6)
C9	0.5368 (4)	−0.1050 (3)	0.34988 (18)	0.0373 (7)
H9A	0.579009	−0.063645	0.409822	0.056*
H9B	0.634031	−0.155031	0.320517	0.056*
H9C	0.418553	−0.173587	0.345406	0.056*
C10	0.2161 (4)	0.1821 (3)	0.45146 (16)	0.0258 (6)
C11	0.6456 (4)	0.3086 (3)	0.06544 (16)	0.0311 (6)
C12	0.4606 (4)	0.2599 (3)	0.07821 (18)	0.0374 (7)
C13	0.3495 (4)	0.3539 (3)	0.12138 (18)	0.0364 (7)
C14	0.4226 (4)	0.4977 (3)	0.15294 (16)	0.0305 (6)
C15	0.6086 (4)	0.5459 (3)	0.14003 (17)	0.0316 (6)
C16	0.7179 (4)	0.4530 (3)	0.09641 (17)	0.0315 (6)
C17	0.2471 (4)	0.6855 (3)	0.16635 (17)	0.0307 (6)
C18	0.0764 (4)	0.8572 (3)	0.17797 (18)	0.0345 (7)
C19	−0.1149 (5)	1.0382 (3)	0.1883 (3)	0.0610 (10)
H19A	−0.017221	1.101278	0.167413	0.092*
H19B	−0.183562	1.096947	0.230976	0.092*
H19C	−0.203541	0.980919	0.140994	0.092*
C20	0.2116 (4)	0.7792 (3)	0.05912 (18)	0.0322 (6)
F1	0.2200 (2)	0.81948 (18)	0.54274 (11)	0.0482 (5)
F2	0.4177 (2)	0.61428 (19)	0.46579 (12)	0.0499 (5)
F3	−0.0880 (3)	0.41263 (19)	0.26064 (10)	0.0501 (5)
F4	−0.2852 (2)	0.61680 (19)	0.33718 (10)	0.0475 (5)
F5	0.3847 (3)	0.12112 (17)	0.04626 (13)	0.0623 (6)
F6	0.1679 (2)	0.30503 (18)	0.13105 (13)	0.0541 (5)
F7	0.6813 (2)	0.68678 (17)	0.16853 (11)	0.0461 (5)
F8	0.8964 (2)	0.50253 (18)	0.08165 (11)	0.0465 (5)
N1	0.1923 (3)	0.2948 (2)	0.42308 (13)	0.0265 (5)
N2	0.3882 (3)	0.2074 (2)	0.31248 (14)	0.0321 (5)
N3	0.3139 (3)	0.0802 (2)	0.41949 (13)	0.0280 (5)
N4	0.2903 (3)	0.6847 (2)	0.08793 (13)	0.0283 (5)
N5	0.1441 (3)	0.7670 (2)	0.21600 (14)	0.0344 (6)

N6	0.1023 (3)	0.8675 (2)	0.09876 (16)	0.0383 (6)
O1	0.2731 (3)	0.4108 (2)	0.31921 (12)	0.0364 (5)
O2	0.5057 (3)	0.00888 (19)	0.31135 (12)	0.0347 (5)
O3	0.1319 (3)	0.16776 (19)	0.52332 (11)	0.0324 (5)
O4	0.3142 (3)	0.58860 (19)	0.20191 (11)	0.0342 (5)
O5	−0.0266 (3)	0.9427 (2)	0.22636 (14)	0.0444 (5)
O6	0.2438 (3)	0.7868 (2)	−0.02171 (12)	0.0382 (5)

Atomic displacement parameters (Å²)

	U^{11}	U^{22}	U^{33}	U^{12}	U^{13}	U^{23}
C1	0.0333 (16)	0.0314 (14)	0.0310 (14)	0.0157 (11)	0.0154 (12)	0.0181 (12)
C2	0.0325 (16)	0.0320 (14)	0.0357 (16)	0.0068 (11)	0.0065 (12)	0.0098 (13)
C3	0.0233 (15)	0.0412 (16)	0.0426 (17)	0.0114 (12)	0.0075 (12)	0.0198 (14)
C4	0.0375 (17)	0.0327 (14)	0.0318 (15)	0.0189 (12)	0.0168 (12)	0.0189 (12)
C5	0.0440 (18)	0.0348 (15)	0.0230 (14)	0.0154 (12)	0.0061 (12)	0.0080 (12)
C6	0.0294 (16)	0.0426 (16)	0.0313 (15)	0.0162 (12)	0.0041 (12)	0.0156 (13)
C7	0.0310 (16)	0.0351 (15)	0.0296 (14)	0.0147 (12)	0.0053 (12)	0.0131 (12)
C8	0.0257 (15)	0.0291 (14)	0.0273 (14)	0.0111 (11)	−0.0001 (11)	0.0035 (11)
C9	0.0459 (19)	0.0319 (15)	0.0392 (16)	0.0210 (13)	0.0081 (14)	0.0089 (13)
C10	0.0238 (14)	0.0305 (14)	0.0254 (13)	0.0080 (10)	0.0030 (11)	0.0094 (11)
C11	0.0361 (17)	0.0369 (15)	0.0253 (14)	0.0139 (12)	0.0089 (12)	0.0117 (12)
C12	0.0448 (19)	0.0270 (14)	0.0401 (16)	0.0047 (12)	0.0131 (14)	0.0082 (13)
C13	0.0297 (16)	0.0408 (16)	0.0406 (16)	0.0026 (12)	0.0152 (13)	0.0149 (13)
C14	0.0335 (16)	0.0378 (15)	0.0240 (13)	0.0108 (12)	0.0083 (12)	0.0114 (12)
C15	0.0325 (16)	0.0342 (15)	0.0282 (14)	0.0041 (12)	0.0037 (12)	0.0093 (12)
C16	0.0224 (15)	0.0432 (16)	0.0313 (14)	0.0047 (12)	0.0051 (11)	0.0144 (12)
C17	0.0268 (15)	0.0313 (14)	0.0345 (15)	0.0021 (11)	0.0056 (12)	0.0110 (12)
C18	0.0300 (16)	0.0286 (14)	0.0405 (17)	0.0020 (11)	0.0133 (13)	0.0017 (13)
C19	0.064 (2)	0.0414 (18)	0.090 (3)	0.0282 (17)	0.042 (2)	0.0258 (19)
C20	0.0298 (16)	0.0311 (14)	0.0369 (16)	0.0055 (11)	0.0085 (12)	0.0100 (12)
F1	0.0395 (11)	0.0452 (10)	0.0525 (11)	0.0088 (8)	0.0003 (8)	−0.0022 (8)
F2	0.0295 (10)	0.0610 (11)	0.0607 (12)	0.0191 (8)	0.0009 (8)	0.0115 (9)
F3	0.0550 (12)	0.0573 (11)	0.0366 (10)	0.0278 (9)	0.0007 (8)	−0.0016 (8)
F4	0.0413 (11)	0.0630 (11)	0.0412 (10)	0.0298 (8)	−0.0030 (8)	0.0059 (8)
F5	0.0613 (13)	0.0313 (9)	0.0865 (15)	0.0000 (8)	0.0327 (11)	0.0035 (9)
F6	0.0368 (11)	0.0478 (10)	0.0715 (13)	−0.0016 (8)	0.0238 (9)	0.0078 (9)
F7	0.0416 (11)	0.0374 (9)	0.0515 (11)	−0.0015 (7)	0.0097 (8)	0.0015 (8)
F8	0.0291 (10)	0.0523 (10)	0.0527 (11)	0.0030 (7)	0.0112 (8)	0.0055 (8)
N1	0.0250 (12)	0.0324 (12)	0.0281 (12)	0.0119 (9)	0.0078 (9)	0.0138 (10)
N2	0.0359 (14)	0.0361 (13)	0.0314 (12)	0.0192 (10)	0.0106 (10)	0.0127 (10)
N3	0.0294 (13)	0.0298 (12)	0.0276 (12)	0.0129 (9)	0.0062 (9)	0.0072 (9)
N4	0.0261 (12)	0.0329 (12)	0.0277 (12)	0.0058 (9)	0.0066 (9)	0.0104 (10)
N5	0.0341 (14)	0.0331 (12)	0.0349 (13)	0.0063 (10)	0.0116 (11)	0.0055 (10)
N6	0.0361 (15)	0.0337 (13)	0.0495 (15)	0.0115 (10)	0.0169 (12)	0.0143 (11)
O1	0.0456 (13)	0.0429 (11)	0.0356 (11)	0.0283 (9)	0.0208 (9)	0.0227 (9)
O2	0.0391 (12)	0.0358 (10)	0.0352 (10)	0.0214 (8)	0.0112 (9)	0.0101 (8)
O3	0.0393 (12)	0.0346 (10)	0.0320 (10)	0.0198 (8)	0.0145 (8)	0.0151 (8)

O4	0.0383 (12)	0.0391 (11)	0.0298 (10)	0.0138 (8)	0.0127 (8)	0.0117 (8)
O5	0.0444 (13)	0.0343 (11)	0.0563 (13)	0.0138 (9)	0.0244 (10)	0.0084 (10)
O6	0.0424 (13)	0.0426 (11)	0.0393 (11)	0.0204 (9)	0.0160 (9)	0.0187 (9)

Geometric parameters (Å, º)

C1—C2	1.378 (4)	C11—C12	1.374 (4)
C1—C6	1.378 (4)	C11—C16	1.378 (4)
C1—O3^{i}	1.390 (3)	C11—O6^{ii}	1.390 (3)
C2—F1	1.336 (3)	C12—F5	1.338 (3)
C2—C3	1.378 (4)	C12—C13	1.381 (4)
C3—F2	1.341 (3)	C13—F6	1.340 (3)
C3—C4	1.368 (4)	C13—C14	1.374 (4)
C4—C5	1.379 (4)	C14—C15	1.380 (4)
C4—O1	1.385 (3)	C14—O4	1.386 (3)
C5—F3	1.344 (3)	C15—F7	1.344 (3)
C5—C6	1.374 (4)	C15—C16	1.368 (4)
C6—F4	1.343 (3)	C16—F8	1.343 (3)
C7—N2	1.311 (3)	C17—N5	1.313 (3)
C7—N1	1.333 (3)	C17—N4	1.321 (3)
C7—O1	1.360 (3)	C17—O4	1.365 (3)
C8—O2	1.325 (3)	C18—O5	1.326 (3)
C8—N3	1.337 (3)	C18—N6	1.335 (4)
C8—N2	1.341 (3)	C18—N5	1.336 (4)
C9—O2	1.447 (3)	C19—O5	1.452 (4)
C10—N3	1.316 (3)	C20—N6	1.317 (3)
C10—N1	1.324 (3)	C20—N4	1.325 (3)
C10—O3	1.358 (3)	C20—O6	1.361 (3)
C2—C1—C6	119.0 (2)	F6—C13—C14	119.7 (2)
C2—C1—O3^{i}	120.8 (2)	F6—C13—C12	119.7 (2)
C6—C1—O3^{i}	120.2 (2)	C14—C13—C12	120.6 (3)
F1—C2—C3	120.0 (2)	C13—C14—C15	118.6 (2)
F1—C2—C1	119.8 (2)	C13—C14—O4	119.9 (2)
C3—C2—C1	120.2 (3)	C15—C14—O4	121.4 (2)
F2—C3—C4	119.5 (2)	F7—C15—C16	119.7 (2)
F2—C3—C2	119.5 (3)	F7—C15—C14	119.5 (2)
C4—C3—C2	121.0 (3)	C16—C15—C14	120.8 (3)
C3—C4—C5	118.7 (2)	F8—C16—C15	120.1 (2)
C3—C4—O1	121.4 (2)	F8—C16—C11	119.1 (2)
C5—C4—O1	119.8 (2)	C15—C16—C11	120.8 (3)
F3—C5—C6	119.0 (2)	N5—C17—N4	128.7 (3)
F3—C5—C4	120.2 (2)	N5—C17—O4	114.0 (2)
C6—C5—C4	120.8 (2)	N4—C17—O4	117.3 (2)
F4—C6—C5	119.8 (2)	O5—C18—N6	119.2 (3)
F4—C6—C1	119.9 (2)	O5—C18—N5	114.1 (2)
C5—C6—C1	120.3 (2)	N6—C18—N5	126.7 (2)
N2—C7—N1	128.8 (2)	N6—C20—N4	128.0 (3)

N2—C7—O1	114.3 (2)	N6—C20—O6	114.7 (2)
N1—C7—O1	116.9 (2)	N4—C20—O6	117.3 (2)
O2—C8—N3	119.5 (2)	C10—N1—C7	111.6 (2)
O2—C8—N2	113.1 (2)	C7—N2—C8	111.6 (2)
N3—C8—N2	127.4 (2)	C10—N3—C8	112.1 (2)
N3—C10—N1	128.4 (2)	C17—N4—C20	111.8 (2)
N3—C10—O3	114.1 (2)	C17—N5—C18	112.2 (2)
N1—C10—O3	117.4 (2)	C20—N6—C18	112.5 (2)
C12—C11—C16	118.7 (2)	C7—O1—C4	116.5 (2)
C12—C11—O6^{ii}	120.2 (2)	C8—O2—C9	117.8 (2)
C16—C11—O6^{ii}	121.1 (2)	C10—O3—C1^{i}	115.88 (19)
F5—C12—C11	120.0 (2)	C17—O4—C14	117.4 (2)
F5—C12—C13	119.4 (3)	C18—O5—C19	117.7 (2)
C11—C12—C13	120.6 (2)	C20—O6—C11^{ii}	115.5 (2)

C6—C1—C2—F1	−176.9 (2)	C12—C11—C16—F8	−177.7 (2)
O3^{i}—C1—C2—F1	4.7 (4)	O6^{ii}—C11—C16—F8	2.0 (4)
C6—C1—C2—C3	0.2 (4)	C12—C11—C16—C15	0.9 (4)
O3^{i}—C1—C2—C3	−178.1 (2)	O6^{ii}—C11—C16—C15	−179.4 (2)
F1—C2—C3—F2	−1.2 (4)	N3—C10—N1—C7	−0.5 (4)
C1—C2—C3—F2	−178.3 (2)	O3—C10—N1—C7	178.7 (2)
F1—C2—C3—C4	177.2 (2)	N2—C7—N1—C10	0.7 (4)
C1—C2—C3—C4	0.0 (4)	O1—C7—N1—C10	−179.0 (2)
F2—C3—C4—C5	178.1 (2)	N1—C7—N2—C8	−0.8 (4)
C2—C3—C4—C5	−0.2 (4)	O1—C7—N2—C8	178.9 (2)
F2—C3—C4—O1	−5.4 (4)	O2—C8—N2—C7	−178.1 (2)
C2—C3—C4—O1	176.3 (2)	N3—C8—N2—C7	0.8 (4)
C3—C4—C5—F3	−179.5 (2)	N1—C10—N3—C8	0.6 (4)
O1—C4—C5—F3	4.0 (4)	O3—C10—N3—C8	−178.7 (2)
C3—C4—C5—C6	0.1 (4)	O2—C8—N3—C10	178.2 (2)
O1—C4—C5—C6	−176.4 (2)	N2—C8—N3—C10	−0.7 (4)
F3—C5—C6—F4	0.9 (4)	N5—C17—N4—C20	−1.4 (4)
C4—C5—C6—F4	−178.6 (2)	O4—C17—N4—C20	177.6 (2)
F3—C5—C6—C1	179.8 (2)	N6—C20—N4—C17	0.0 (4)
C4—C5—C6—C1	0.2 (4)	O6—C20—N4—C17	−179.1 (2)
C2—C1—C6—F4	178.5 (2)	N4—C17—N5—C18	0.9 (4)
O3^{i}—C1—C6—F4	−3.2 (4)	O4—C17—N5—C18	−178.1 (2)
C2—C1—C6—C5	−0.4 (4)	O5—C18—N5—C17	−179.2 (2)
O3^{i}—C1—C6—C5	178.0 (2)	N6—C18—N5—C17	1.0 (4)
C16—C11—C12—F5	177.6 (3)	N4—C20—N6—C18	1.5 (4)
O6^{ii}—C11—C12—F5	−2.1 (4)	O6—C20—N6—C18	−179.3 (2)
C16—C11—C12—C13	−0.1 (4)	O5—C18—N6—C20	178.2 (2)
O6^{ii}—C11—C12—C13	−179.8 (3)	N5—C18—N6—C20	−2.1 (4)
F5—C12—C13—F6	0.3 (4)	N2—C7—O1—C4	−178.1 (2)
C11—C12—C13—F6	178.1 (3)	N1—C7—O1—C4	1.6 (4)
F5—C12—C13—C14	−178.3 (3)	C3—C4—O1—C7	79.5 (3)
C11—C12—C13—C14	−0.5 (4)	C5—C4—O1—C7	−104.1 (3)
F6—C13—C14—C15	−178.2 (2)	N3—C8—O2—C9	−3.4 (4)

C12—C13—C14—C15	0.4 (4)	N2—C8—O2—C9	175.6 (2)
F6—C13—C14—O4	6.5 (4)	N3—C10—O3—C1^{i}	178.0 (2)
C12—C13—C14—O4	−174.9 (3)	N1—C10—O3—C1^{i}	−1.3 (3)
C13—C14—C15—F7	178.3 (2)	N5—C17—O4—C14	179.3 (2)
O4—C14—C15—F7	−6.5 (4)	N4—C17—O4—C14	0.2 (3)
C13—C14—C15—C16	0.3 (4)	C13—C14—O4—C17	−108.6 (3)
O4—C14—C15—C16	175.5 (2)	C15—C14—O4—C17	76.3 (3)
F7—C15—C16—F8	−0.5 (4)	N6—C18—O5—C19	3.3 (4)
C14—C15—C16—F8	177.5 (2)	N5—C18—O5—C19	−176.5 (3)
F7—C15—C16—C11	−179.0 (2)	N6—C20—O6—C11^{ii}	−178.2 (2)
C14—C15—C16—C11	−1.0 (4)	N4—C20—O6—C11^{ii}	1.0 (3)

Symmetry codes: (i) −*x*, −*y*+1, −*z*+1; (ii) −*x*+1, −*y*+1, −*z*.